Modelling the photosphere of active stars for planet detection and characterization

Enrique Herrero[1]**, Ignasi Ribas**[1]**, Carme Jordi**[2]**, Juan Carlos Morales**[3]**, Manuel Perger**[1]**, and Albert Rosich**[1]

[1] Institut de Ciències de l'Espai (CSIC-IEEC)
[2] Dept. d'Astronomia i Meteorologia, Institut de Ciències del Cosmos (ICC)
[3] LESIA-Observatoire de Paris

Abstract

Stellar activity patterns are responsible for jitter effects that are observed at different timescales and amplitudes in the measurements obtained from photometric and spectroscopic time series observations. These effects are usually considered just noise, and the lack of a characterization and correction strategy represents one of the main limitations to detect the signals of small exoplanets. Accurate simulations of the stellar photosphere based on the most recent available models for main sequence stars can provide synthetic photometric and spectroscopic time series data. These may help to investigate the relation between activity jitter and stellar parameters when considering different active region patterns. Moreover, jitters can be analysed at different wavelength scales (defined by the passbands of given instruments or space missions) in order to design strategies to remove or minimize them. In this work we present the StarSim tool, which is based on a model for a spotted rotating photosphere built from the integration of the spectral contribution of a fine grid of surface elements, including all significant effects affecting the flux intensities and the wavelength of spectral features produced by active regions and transiting planets.

1 Introduction

Stellar activity in late-type main sequence stars induces photometric modulations and apparent radial velocity variations that may hamper the detection of Earth-like planets ([9, 11]) and the measurement of their transit parameters ([3]), mass and atmospheric properties. A frequently tacit assumption when modelling light and radial velocity curves is that any temporal variation in the calibrated signal from the (unresolved) host star/exoplanet can be attributed to changes in the (small) signal from the exoplanet, and is not a result of variation in either the stellar signal or instrument response.

Late-type stars (i.e., late-F, G, K and M spectral types) are known to be variable to some extent. The effect of activity in the stellar photosphere is seen in the form of spots and faculae, whose relationship with parameters such as mass and age is still not well understood. The signal of these activity patterns is modulated by the stellar rotation period. Such effects need to be subtracted or accounted for the design of planet search strategies ([7, 8, 12]).

Significant improvement in our knowledge of activity effects on starlight will be crucial to make the most of present and future planet search spectrographs (HARPS-N & S, CARMENES, ESPRESSO, HIRES, APF) and transit observations from space (CHEOPS, PLATO, JWST). The most up-to-date and comprehensive information on stellar variability comes from the studies with the Kepler mission, which are based on the observation and analysis of ∼150,000 stars taken from the first Kepler data release. [6] have found that 80% of M dwarfs have light dispersion less than 500 ppm over a period of 12 hours, while G dwarfs are the most stable group down to 40 ppm. Kepler operates in the visible (430 to 890 nm) where stellar photometric variability is a factor of 2 or more higher than in the near and thermal IR (the "sweet spot" for the characterization of exoplanet atmospheres). [10] investigate the variability properties of main sequence stars in the Kepler data, finding that the typical amplitude and time-scale increase towards later spectral types, which could be related to an increase in the characteristic size and life-time of active regions.

2 Simulation of the photosphere of active stars

A methodology to simulate spectra from the spotted photosphere of a rotating star has been developed and is presented as the StarSim tool. We use atmosphere models for low mass stars to generate synthetic spectra for the stellar surface, spots and faculae. The spectrum of the entire visible face of the star is obtained from the contribution of a grid of small surface elements. Using such simulator, time series spectra can be obtained covering the rotation period the star or longer. By convolving these with the known bandpass for a specific instrument, they can be used to study the chromatic effects of spots and faculae on photometric modulation and radial velocity jitter.

Among the most recent model atmosphere grids, we use spectra from the BT-Settl database [1] generated with the Phoenix code in order to reproduce the spectral signal for every element in the photosphere. These models include revised solar oxygen abundances and cloud model, which allow reproducing the photometric and spectroscopic properties also in very low mass stars.

As said, the stellar photosphere is divided into a grid of surface elements. The spatial resolution of the grid is a parameter, and $1° \times 1°$ size elements have been tested to correctly reproduce most active region configurations and transiting planet effects up to $\sim 10^{-6}$ photometric precision. Three models with different temperatures are considered in order to build the stellar spectrum: quiet photosphere, spots and faculae. The active regions map is specified as a list of coordinates, radii and lifetimes describing each active region. Our model does not distinguish between umbra and penumbra, but adopts a mean spot contrast at an intermediate temperature, as adopted by previous approaches [5] [14]. Active region evolu-
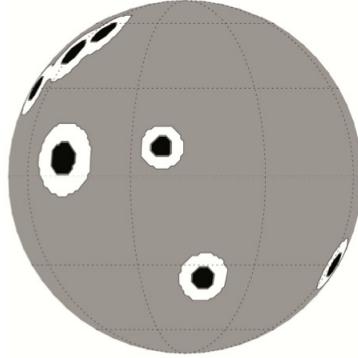
Figure 1: Projected map for an arbitrarily generated distribution of active regions. The quiet photosphere is represented in grey, and each active region is modeled as a cold spot (black) and a hotter surrounding area to account for faculae (white).

tion (i.e., changes in size over time) is modeled as a lineal rise period followed by a constant size time and a final decay. Each active region n is modeled as a circular spot of radius R_{Sn} surrounded by a facula with a coronal shape, having an external radius $R_{Fn} = \sqrt{Q+1} \cdot R_{Sn}$ (see Fig. 1).

The differential rotation of the star is modeled considering:

$$P(\phi) = P_0 + k_{rot} \cdot P_{\text{Sun}} \cdot \sin^2\theta, \qquad P_{\text{Sun}} = 3.1913°/\text{day}, \tag{1}$$

where the equatorial rotation period P_0 and the differential rotation factor k_{rot} are specified as input parameters, and θ is the variable denoting the latitude. Also, the inclination of the stellar axis towards the observer is a parameter and can vary from $0°$ to $90°$.

Together with the physical parameters of the star- planet system, the spectral range for the output data, and the time span and cadence of the data series can be adjusted. The program also creates a light curve by convolving each created spectrum with a specified filter bandpass. Finally, the integration time, the telescope collecting area, the response of the detector and the target star magnitude need to be specified in order to apply photon noise statistics to the resulting fluxes.

The program reads the physical parameters for the three photospheric features of the modeled star (quiet photosphere, spots and faculae) and interpolates within the corresponding model atmosphere grids to generate the three synthetic spectra: $f_p(\lambda)$, $f_s(\lambda)$ and $f_f(\lambda)$. Also, Kurucz (ATLAS9) spectra [4] are generated for the same parameters for the photosphere, spots and faculae, as these models provide information on the limb darkening profile function $I(\lambda, \mu)/I(\lambda, 0)$.

First, the spectrum for an immaculate photosphere is obtained from the contribution of all the surface elements, taking into account the geometry of the element, its projection towards the observer, its limb darkening function and its radial velocity shift:

$$f_{im}(\lambda) \;=\; \sum_k f_p(\lambda + \Delta\lambda_k, \mu_k, a_k) =$$

$$=\; \sum_k f_p(\lambda + \Delta\lambda_k) \otimes \frac{I_p(\lambda, \mu_k)}{I_p(\lambda, 0)} \cdot a_k \cdot \mu_k \cdot \omega_k, \tag{2}$$

where k denotes the surface element and μ_k is its projection angle given by

$$\mu_k = \sin i \sin\theta_k \cos\phi_k + \cos i \cos\theta_k. \tag{3}$$

ϕ_k and ω_k are the longitude and latitude coordinates of the surface element, respectively, and the factor ω_k accounts for its visibility, which is 1 and 0 for $\mu_k \geq 0$ and $\mu_k < 0$, respectively. a_k is the area of the surface element, which can be computed from their size (the resolution of the surface grid, $\Delta\alpha$) by

$$a_k = 2 \cdot \Delta\alpha \cdot \sin(\frac{\Delta\alpha}{2}) \sin\theta_k. \tag{4}$$

Finally, $\Delta\lambda$ are the Doppler shifts added to the wavelength vector,

$$\Delta\lambda_k = -8.05 \cdot \lambda \cdot \frac{1}{c} \cdot R_{\text{star}} \cdot \frac{2\pi}{P_{\text{rot}}} \sin i \sin\theta_k \sin\phi_k. \tag{5}$$

in km s^{-1}, where the rotation period P_{rot} (in days) is given in the input parameters and the stellar radius R_{star} (in units of $R_\odot$) is calculated using its relation with $\log g$ and T_{eff}.

The flux variations Δf_j^{ar} produced by the visible active regions are added to the contribution of the immaculate photosphere when computing the spectrum at each time step j. These are given by

$$\Delta f_j^{\text{ar}}(\lambda) =$$

$$=\; \sum_k [(f_s(\lambda + \Delta\lambda_k) - f_p(\lambda + \Delta\lambda_k)) \otimes \frac{I_s(\lambda, \mu_{kj})}{I_s(\lambda, 0)} \cdot a_k \cdot \mu_{kj} \cdot \omega_k \cdot p_{kj}^s +$$

$$+\; (f_f(\lambda + \Delta\lambda_k) - f_p(\lambda + \Delta\lambda_k)) \cdot c_f(\mu_{kj}) \cdot a_k \cdot \mu_{kj} \cdot \omega_k \cdot p_{kj}^f], \tag{6}$$

where the first term accounts for the flux deficit produced by the spots and the second is the overflux introduced by the faculae. The factors p_{kj}^s and p_{kj}^f are the fractions of the surface element k covered by spot and facula, respectively. These amounts are calculated for every surface element considering their distance to the center of all the near active regions at each observation j. $c_f(\mu_k)$ accounts for the limb brightening of faculae [13] [2]. There is also a time dependence of the projection of the surface elements, given by

$$\mu_{kj} = \sin i \sin\theta_k \cos[\phi_k + \omega(t_j - t_0)] + \cos i \cos\theta_k. \tag{7}$$
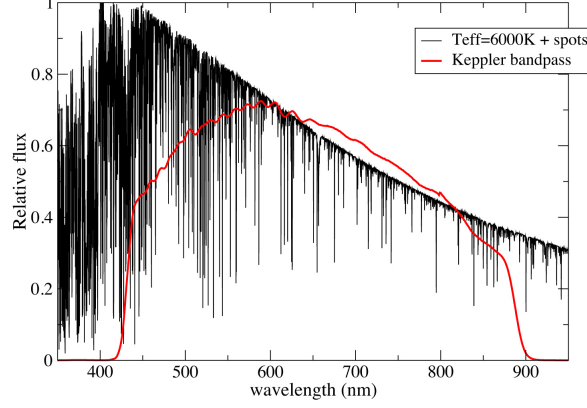
Figure 2:   Normalized flux for a simulated spectrum for a Sun-like star with several active regions generated from BT-Settl model spectra (black). In red, the transmission function of the Kepler filter.

One or more transiting planets can be introduced in the simulations. Each transiting planet is considered as a dark circular spot, with a no radius dependence on wavelength (no atmosphere), crossing the stellar disk. For each time step j, the planet position is obtained from the given ephemeris and the flux deficit Δf_j^{tr} is computed from the occulted surface elements of the star:

$$\Delta f_j^{\mathrm{tr}}(\lambda) = -\sum_k f_{\mathrm{p}}(\lambda + \Delta\lambda_k) \otimes \frac{I_{\mathrm{s}}(\lambda, \mu_{kj})}{I_{\mathrm{s}}(\lambda, 0)} \cdot a_k \cdot \mu_{kj} \cdot \omega_k \cdot p_{kj}^{\mathrm{tr}}, \tag{8}$$

where p_{kj}^{tr} is the fraction of the surface element k covered by the planet.

Finally, the spectrum for the observation j is obtained by adding the contribution of the immaculate photosphere, the active regions and the transiting planet:

$$f_j(\lambda) = f_{\mathrm{im}}(\lambda) + \Delta f_j^{\mathrm{ar}}(\lambda) + \Delta f_j^{\mathrm{tr}}(\lambda). \tag{9}$$

The resulting time series spectra are convolved with the specified filter bandpass (see Fig. 2) in order to obtain a light curve and further study the photometric jitter produced by activity at the desired spectral ranges.

3   Discussion and conclusions

We present a methodology, in the form of the StarSim tool, to simulate the photosphere of rotating spotted stars. This allows us to generate synthetic photometric and spectroscopic time series data from a set of given parameters and a library of atmosphere stellar models.

The main purposes of this methodology are the characterization of the effects produced by activity in time series observations, especially multi-band studies of exoplanetary transits, and the design of strategies for the minimization of activity effects, both when searching and characterizing exoplanets.

The approach presented in this paper accurately accounts for all the physical processes produced by activity, which currently represents the main obstacle for exoplanet characterization and searches. In fact, our approach can help to model and correct for the effects of activity jitter on photometric and radial velocity observations of extrasolar planets. Also, our simulations allow studying the effects of the amount of faculae as well as of spot temperature contrasts and sizes on multi-band simultaneous photometry. The methodology is currently being implemented in a more efficient way to model fit multi-band photometric and spectroscopic radial velocity observations simultaneously, thus obtaining detailed maps for the characterization of stellar photospheres. Several applications of the methodology to real observations and to the design of optimized strategies for the search and characterization of exoplanets will be presented in a series of papers in the near future. Stellar activity needs to be properly accounted for in order to be able to detect and understand the atmospheres of small planets.

Acknowledgments

References

[1] Allard, F., Homeier, D., Freytag, B., et al. 2013, MmSAI, 24, 128

[2] Ball, W. T., Unruh, Y. C., Krivova, N. A. et al. 2011, A&A, 530, A71

[3] Barros, S. C. C., Bou, G., Gibson, N. P., et al. 2013, MNRAS, 430, 3032

[4] Castelli, F. & Kurucz, R. L. 2004, arXiv:astro-ph/0405087

[5] Chapman, G. A. 1987, ARA&A, 25, 633

[6] Ciardi, D. R., von Braun, K., Bryden, G., et al. 2011, AJ, 141, 108

[7] Dumusque, X., Santos, N. C., Udry, S., Lovis, C., & Bonfils, X. 2011a, A&A, 527, A82

[8] Dumusque, X., Udry, S., Lovis, C. et al. 2011b, A&A, 525, A140

[9] Lagrange, A.-M., Desort, M., Meunier, N. 2010, A&A, 512, A38

[10] McQuillan, A., Aigrain, S., Roberts, S. 2012, A&A, 539, A137

[11] Meunier, N., Desort, M., Lagrange, A.-M. 2010a, A&A, 512, A39

[12] Moulds, V. E., Watson, C. A., Bonfils, X. et al. 2013, MNRAS, 430, 1709

[13] Ortiz, A., Solanki, S. K., Domingo, V. et al. 2002, A&A, 388, 1036

[14] Unruh, Y. C., Solanki, S. K., Fligge, M. 1999, A&A, 345, 635